ELSEVIER

Journal of Marine Systems 22 (1999) 105–116

JOURNAL OF MARINE SYSTEMS

Hydrodynamic and sediment suspension modelling in estuarine systems Part I: Description of the numerical models

Leonor Cancino, Ramiro Neves *

Instituto Superior Técnico, Department of Mechanical Engineering, Av. Rovisco Pais, P-1096 Lisbon, Portugal

Received 15 October 1996; accepted 1 November 1998

Abstract

A fully-3D finite difference baroclinic model system for hydrodynamics and fine suspended sediment transport is described. The hydrodynamic model is based on the hydrostatic and Boussinesq approximations, and uses a vertical double sigma co-ordinate with a staggered grid and a semi-implicit two-time level scheme. In addition to the momentum and continuity equations, the model solves two transport equations for salt and temperature and an equation of state to include the baroclinic effects. The simulation of cohesive sediment transport processes is performed solving the 3D-conservative advection–diffusion equation, in the same grid used by the hydrodynamic model. Flocculation, erosion and deposition of sediments on the bottom are represented by means of empirical formulations parameterized by field data. The models were tested and calibrated by simulating tidal flows and suspended sediment transport in several estuaries (two applications are described in Part II). The results show good agreement between the numerical predictions and the corresponding field measurements.

Keywords: hydrodynamic suspension; estuarine systems; numerical models

1. Introduction

The filtering role of estuaries makes them crucial transitional areas trapping significant quantities of particulate and dissolved matter through a wide variety of physical and biogeochemical processes. Cohesive sediments play an important role in these processes. Unlike sand, well characterised by its grain size distribution, cohesive sediments are complex mixtures of different clay minerals—mainly illite, montmorillonite and kaolinite—organic matter and a small percentage of sand and silt.

Hydrodynamic action is the most important mechanism involved in sediment transport. It advects the suspended sediments, provides the force need to erode the bed and, through turbulence, plays a major role in the flocculation of cohesive sediments. Relatively large velocities generally occur in tidal estuaries. Because the hydrodynamic processes involved in sediment transport are mainly non-linear, the sediments are very mobile in these estuaries. They are eroded and transported upwards during flood, deposited during slack water, eroded again and trans-

* Corresponding author. E-mail: ramiro.neves@hidrox.ist.utl.pt

0924-7963/99/$ - see front matter
PII: S0924-7963(99)00035-4

ported downwards during ebb and redeposited during next slack water, to restart their movement in the forthcoming tidal cycle.

In tidal estuaries the amount of sediments in movement can be very large but, due to its oscillating nature, the net sediment transport can be very small. So, time scales of bottom evolution should be expected to be much larger than a tidal period. For these reasons, the field study of sediment transport is very difficult. If the tidal period is chosen as the time scale, the mechanisms and the detailed motion of the sediments can be studied. On the other hand, for longer time scales, the study can yield the monitoring of net erosion/deposition of sediments. Short-term processes are frequently a concern of Coastal Engineering, whereas the long-term evolution is mainly a matter of geological studies. Mathematical modelling can be a bridge between them.

The first attempt to correlate sediment transport and fluid dynamics is due to Bagnold (1936, 1937). He was a soldier during the First World War, placed in duty in the Egyptian Sahara desert. The frequent sandstorms drove his interest on the subject. The works carried out later by Einstein (1950) and his collaborators, and the development of the computing capacity, turned the mathematical modelling of sediment transport into a major subject in coastal sciences.

Cohesive and non-cohesive sediments are different from each other in two major aspects: flocculation and consolidation of deposited material with compaction of the sediments. Flocs are formed by gluing individual particles and can strongly modify the settling velocity of particulate matter. After bottom deposition, the water content is still a significant part of the bed material. The expulsion of this water is part of the sediment consolidation process. The small pore dimensions imply long times for sediment deposition, which creates conditions for fluid–mud formation in environments with very high availability of sediments.

The long time scale associated with consolidation and the strong dynamics of sediment in tidal estuaries make this process of secondary importance in short-term studies. In an estuary, three types of areas may be considered according to the deposition budget: erosion areas, deposition areas and equilibrium areas. In deposition areas, there are available sediments but the flow cannot erode them. In equilibrium areas, the amount of deposited sediments balances the erosion and there is no place to consolidation. In erosion areas, the important information is the knowledge of the vertical structure of the bed in order to know how the critical shear stress increases as erosion proceeds. In these conditions, consolidation becomes important only in fluid–mud formation or in very long-term simulations (decades) when sediment deposition is able to modify the hydrodynamic regime.

In these conditions, cohesive sediment transport models can be classified into two main groups according to their ability to model the formation and transport of fluid mud. The model presented in this paper does not consider the formation of fluid–mud and can be used only in estuaries with moderate sediment concentrations. Models of this type consider tidal advection, flocculation and the exchanges with the bottom (erosion and deposition). The basic differences among them arise mainly from the number of dimensions considered, the numerical technique adopted, the complexity of the description of the bed and from the effects considered in the hydrodynamic forcing (e.g., tides, density flows, and wind waves). For reasons of computing costs, until recently most applications have been restricted to transport processes in one-dimension (1D) or two-dimension (2D).

One of the earliest studies concerning fluid–mud conditions (Einstein and Chien, 1955) was undertaken dividing the water column into a bed heavy fluid zone with high sediment concentration, and a light fluid zone with lower sediment concentration occupying the remainder of the water column. A velocity distribution was derived for each zone. In this work, both flocculation and bed consolidation were studied. It was verified that a minimum salinity of 1‰ was required for the onset of flocculation. The consolidation was quantified by noting the variation of the bed thickness with time in two different phases and by order of aggregation. More recently, Odd and Owen (1972) developed, along the same lines, a 1D model considering a deeper thin lower layer with constant depth and an upper layer of varying thickness. Erosion and deposition rates were based on the formulations proposed by Krone (1962) and Partheniades (1965). 1D models have been fre-

quently used to simulate sediment transport and large-scale morphological changes in rivers (De Vries et al., 1989), in tidal channels (Dyer and Evans, 1989) and for the simulation of lutocline formation in estuaries (Ross and Mehta, 1989; Smith and Kirby, 1989).

An early 2D vertical integrated model was presented by O'Connor (1971). Other 2D vertical integrated models have followed this one. Ariathurai and Krone (1976) presented a finite element model adopting triangular elements with a quadratic approximation for the concentration and a Galerkian weighted residual method. The model utilises the classical relations for erosion and deposition mentioned above. Flocculation is accounted for by specifying different settling velocities in each element as a function of time. In this work, the authors defend that each clay mineral becomes cohesive at a different salinity value. Mulder and Udink (1991) presented a 2D model for the Western Scheldt estuary (The Netherlands) in which the tide and wind wave models were combined to produce stationary wave fields. The model solves a spectral action balance equation (with interpolation between the calculated wave heights and wave periods at different tidal stages) to determine the orbital velocity and bottom shear stress component due to waves. Classical empirical expressions for sedimentation and erosion were used. Uniform values for critical shear stress of erosion and deposition and constant settling velocity were imposed. Consolidation was neglected.

Li et al. (1994) developed a coupled 2-DV width-integrated hydrodynamic and sediment transport model for the Gironde estuary (France). A turbulent-closure model is described to compute turbulent viscosity and diffusion coefficients. Bottom exchange was calculated based on the classical formulations.

Sediment transport is a three-dimensional (3D) phenomenon. Even if there is no strong density gradient, the settling velocity and the water–bottom interaction generate vertical gradients of suspended sediment. For these reasons, 3D approaches are the most adequate for sediment transport modelling purposes. Nowadays, even with inexpensive computers, these models are feasible and are capable of simulating the tide, wind and density forcing. Important 3D effects are present in regions with strong curvature, generating secondary flows responsible for the accumulation of sediments along the concave side of the estuary domain.

In 3D formulations, the bottom boundary layer can be simulated explicitly. Sheng (1986) discussed the erosion and deposition processes together with the bottom boundary layer model. O'Connor and Nicholson (1988) provided a fully 3D model, including a fluid–mud transport model, flocculation and consolidation. Katopodi and Ribberink (1992) developed a quasi-3D model for suspended sediment transport based on an asymptotic solution of the advection–diffusion equation for currents and waves. A sensitivity analysis of the relative importance of current and wave parameters on the suspended adjustment phenomenon shows that the presence of the latter considerably increases the suspended load and its adjustment time and length scales. The model results are compared with 2D width-integrated and fully 3D numerical solutions. Baroclinic models for hydrodynamic and sediment transport has been developed for coastal zones (De Kok et al., 1995) and for estuaries (Cancino and Neves, 1994a,b; 1995). Applications of the latter to the Western Scheldt and Gironde estuaries are described in Part II of this paper.

2. Hydrodynamic model

2.1. Model equations

The hydrodynamic model used is a fully 3D-baroclinic model. It considers the hydrostatic and Boussinesq approximations, uses a vertical double sigma co-ordinate with a staggered grid and a semi-implicit two-time level scheme (Santos and Neves, 1991; Santos, 1995).

The horizontal transport and the Coriolis term are solved explicitly, while the model uses an implicit algorithm for the pressure terms and for the vertical transport. The horizontal viscosity calculation is based on Kolmogorov's law. The computation of the vertical viscosity is based on a mixing length approach.

Tidal forcing is prescribed at the marine boundary, whereas the flow rate is imposed at the river boundary. At the natural air–sea boundary, the con-

ditions are prescribed by using known-atmospheric values. In addition to the momentum and continuity equations, the model can optionally solve two transport equations for salt and temperature and an equation of state to include the baroclinic effects.

The momentum and continuity equations in Cartesian co-ordinates are:

$$\frac{\partial u}{\partial t}+u\frac{\partial u}{\partial x}+v\frac{\partial u}{\partial y}+w\frac{\partial u}{\partial z}-fv = -\frac{1}{\rho_r}\frac{\partial p}{\partial x}+\frac{\partial}{\partial x}\left(A_H\frac{\partial u}{\partial x}\right)+\frac{\partial}{\partial y}\left(A_H\frac{\partial u}{\partial y}\right)+\frac{\partial}{\partial z}\left(A_V\frac{\partial u}{\partial z}\right), \quad (1)$$

$$\frac{\partial v}{\partial t}+u\frac{\partial v}{\partial x}+v\frac{\partial v}{\partial y}+w\frac{\partial v}{\partial z}+fu = -\frac{1}{\rho_r}\frac{\partial p}{\partial y}+\frac{\partial}{\partial x}\left(A_H\frac{\partial v}{\partial x}\right)+\frac{\partial}{\partial y}\left(A_H\frac{\partial v}{\partial y}\right)+\frac{\partial}{\partial z}\left(A_V\frac{\partial v}{\partial z}\right), \quad (2)$$

$$\frac{\partial p}{\partial z}+\rho g=0, \quad (3)$$

$$\frac{\partial u}{\partial x}+\frac{\partial v}{\partial y}+\frac{\partial w}{\partial z}=0, \quad (4)$$

where t is time, u, v, w are the velocity components in the x, y, z directions, f is the Coriolis parameter, p is pressure, ρ is water density, g is the acceleration of gravity, and A_H and A_V are the horizontal and vertical turbulent viscosities.

At the bottom, the friction shear stress is imposed assuming a logarithmic velocity profile:

$$\tau=c_d|\bar{u}_+|\bar{u}_+, \quad (5)$$

$$c_d=k^2\left(\ln\frac{z_+}{z_0}\right)^{-2}, \quad (6)$$

where: τ is the bed shear stress, u_+ is the horizontal velocity vector at the distance z_+ above the bottom, c_d is bottom drag coefficient, k is the von Karman constant, and z_0 is the physical roughness height.

At the free surface, the flux of momentum is also imposed in the form of a shear stress. The model solves two transport equations for salt and temperature and an equation of state to include the baroclinic effects. The governing transport equations can be written as:

$$\frac{\partial(S)}{\partial t}+\frac{\partial(uS)}{\partial x}+\frac{\partial(vS)}{\partial y}+\frac{\partial(wS)}{\partial z} = \frac{\partial}{\partial x}\left(K_H\frac{\partial S}{\partial x}\right)+\frac{\partial}{\partial y}\left(K_H\frac{\partial S}{\partial y}\right)+\frac{\partial}{\partial z}\left(K_V\frac{\partial S}{\partial z}\right), \quad (7a)$$

$$\frac{\partial(T)}{\partial t}+\frac{\partial(uT)}{\partial x}+\frac{\partial(vT)}{\partial y}+\frac{\partial(wT)}{\partial z} = \frac{\partial}{\partial x}\left(K_H\frac{\partial T}{\partial x}\right)+\frac{\partial}{\partial y}\left(K_H\frac{\partial T}{\partial y}\right)+\frac{\partial}{\partial z}\left(K_V\frac{\partial T}{\partial z}\right), \quad (7b)$$

$$\rho=(5890+38T-0.375T^2+3S)/(1779.5+11.25T-0.0745T^2-(3.8+0.01T)S+0.698(5890+38T+0.375T^2+3S)), \quad (7c)$$

where S and T are salinity and temperature, t is time, x, y are the horizontal co-ordinates, z is the vertical co-ordinate, K_H, K_V are the horizontal and the vertical salinity and heat diffusion coefficients, and u, v, w are the flow velocity components in the x, y, z directions.

In these equations, the bottom boundary condition is zero flux, while at the surface fluxes of heat and water are imposed. At the open boundaries, the diffusive fluxes are neglected. During ebb, no other boundary condition is needed. During flood, a relaxation is imposed for known marine values. The relaxation time is estimated by using field data.

2.2. The simple vertical sigma co-ordinate

The quality of the results of a 3D model that solves Eq. (1)–(4), Eq. (7a–c), depends on its ability to describe the vertical processes. The sigma co-ordinate introduced in meteorology by Phillips (1957), and used in marine systems by a number of authors (Blumberg and Mellor, 1983; Beckers, 1991;

Santos, 1995), allows the same number of layers to be used independently of the local depth.

Fig. 1 (adapted from Cancino and Neves, 1994a) describes how the water column in an irregular (real) topography is dealt with in Cartesian (Fig. 1a,b) and sigma co-ordinates (Fig. 1c,d). In Cartesian co-ordinates, horizontal plane intercept the bottom that is represented by a number of steps. In sigma co-ordinates, the layers follow the topography (Fig. 1c) and equations are solved in a transformed rectangular domain. Some advantages of the sigma co-ordinate can be clearly identified from that figure: shallow regions are better discretised in the sigma plane and the calculation of the bottom shear stress —a major task in a sediment transport model—is more accurate in the sigma model. To achieve the same vertical resolution in shallow areas more layers are needed in the Cartesian grid.

The new vertical co-ordinate x_3 is expressed by:

$$x_3 = \frac{L}{H}(z + h) \qquad \text{with} \quad x_3 \in (0, L), \tag{8a}$$

$$H = \xi + h, \tag{8b}$$

where L is a characteristic length scale, H is the maximum height of the water column, ξ is the elevation of water surface, h the local depth, (positive if the bottom lays below the reference sea level), and z is the vertical Cartesian co-ordinate (positive above the reference sea level).

In the sigma plane, the vertical co-ordinate varies between $x_3 = 0$ at the bottom and $x_3 = L$ at the free surface. The horizontal co-ordinates are identical in both co-ordinate systems.

The sigma co-ordinate is quite convenient whenever the bathymetry plays a major role in the flow.

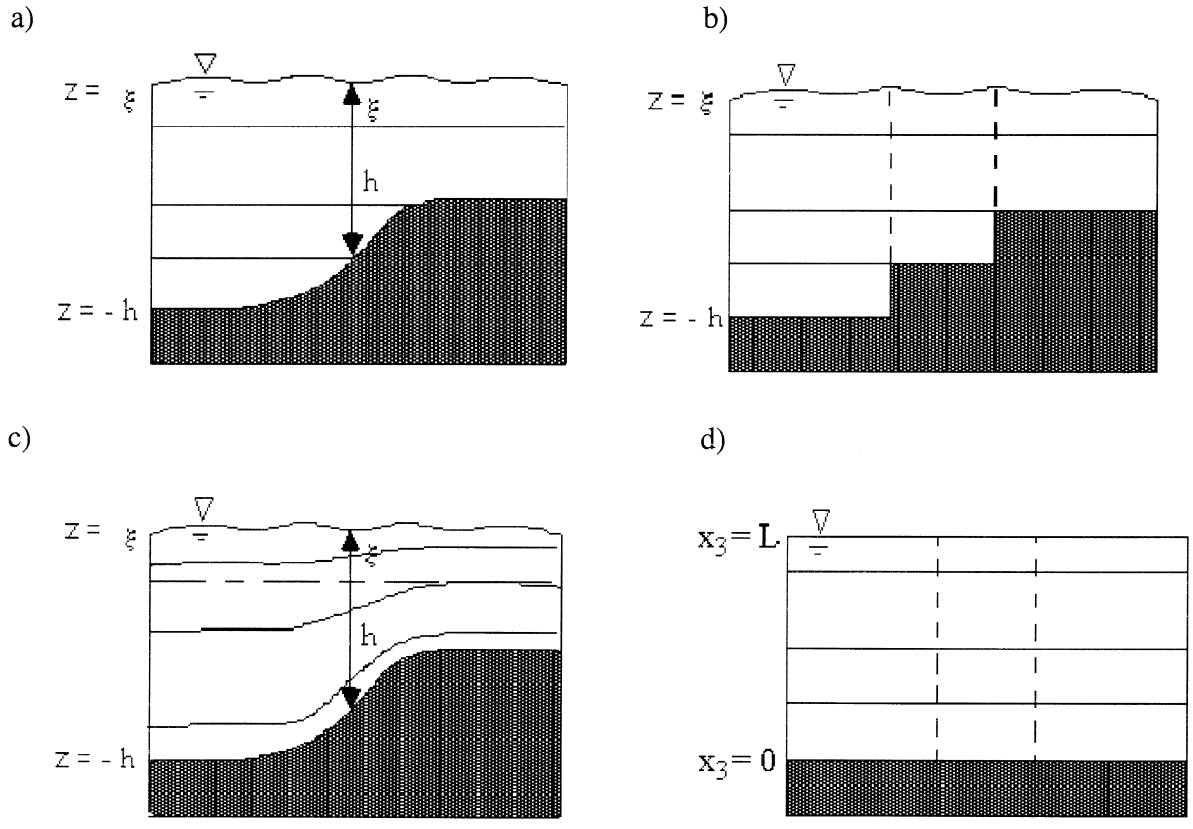

Fig. 1. Representation of an idealised vertical profile (a) in a real domain, (b) in a Cartesian model, (c) in a model using the sigma co-ordinate and (d) in the sigma plane (adapted from Cancino and Neves, 1994a).

This is very often the case in shallow coastal areas, but very seldom in the ocean where density is a major forcing or, through vertical turbulence inhibition, determines the vertical fluxes of momentum and heat across the water column. Even in the shallow areas, intertidal regions are harder to deal with in a simple sigma co-ordinate. A double sigma co-ordinate can minimise both problems.

2.3. The double vertical sigma co-ordinate

The consideration of the same number of layers regardless of the local depth is generally pointed out as a major advantage of this type of co-ordinates. In intertidal areas, during the drying process, as the water height approaches zero the local thickness of the layers becomes very small. In a numerical model, this has direct implications on stability and accuracy, since the time step depends on the courant and diffusion numbers. For that reason, a numerical model must consider a minimum thickness for each layer. In intertidal areas, this implies that the number of layers must be small (1 to 3). This does not arise in practical problems because in intertidal areas the vertical stratification is very weak and there is no need for a vertical discretisation.

A double sigma co-ordinate uses a horizontal plane to split the water column into two vertical domains and considers a sigma transformation in each of them. In regions where the bottom lays below the splitting plane, the two domains exist, while in the shallow areas, only the upper one does. The number of layers is constant in each of the domains. If the splitting plane is close to the minimum water level—e.g., coincident with the hydrographic zero—the number of layers in the intertidal areas is equal to the number of layers of the upper domain. In the limiting case of one layer in the upper domain, intertidal areas are dealt with by a 3D model as in a 2D vertical integrated model and the time step is limited only by the reflected waves associated with the discrete process of moving the drying/flooding boundary. If more than one layer is used in the upper domain, a smaller time step must be used, which, however, is larger than in the case of a simple sigma co-ordinate.

This type of co-ordinate also minimises the lack of ability of the sigma co-ordinate to deal with stratified flows. In these flows, pycnoclines in general are quasi-horizontal and do not follow the bottom topography. Fig. 2a (adapted from Beckers, 1991) shows the sigma grid and a horizontal line representing a pycnocline. Fig. 2b represents the transformed domain and the transformed horizontal line crossing the sigma grid.

In a stratified flow, the velocity over a horizontal pycnocline is horizontal. In the transformed domain the horizontal velocity remains invariant. In the case of Fig. 2b, a horizontal velocity displaces the line leftwards. This corresponds in the real domain to a leftward plus an upward movement, and to a downward movement in the case of a rightward transport. If the property being considered is an active tracer (e.g., temperature or salinity) this artificial movement will modify the vertical distribution of the density and consequently the flow. This error increases with the vertical depth gradient and the horizontal grid step. In case of stratified flows with a clear thermocline, a double sigma co-ordinate can be used with the splitting plane located immediately above the region of larger density gradients (Delleersnijder and Beckers, 1992; Santos, 1995). Fig. 2b and c compare the grids in both co-ordinate systems and show how a horizontal pycnocline is represented in both systems of co-ordinates.

Fig. 2b also puts into evidence that the baroclinic pressure gradient cannot be calculated in the sigma grid. In case of an irregular bathymetry, this would correspond to an integration from the surface until levels corresponding to different real coordinates. Considering a situation where all density gradients are horizontal, it is clear that this procedure would create an artificial horizontal baroclinic gradient and a corresponding flow. The errors again increase with the vertical depth gradient and the horizontal step of the grid. This can only be solved using a Cartesian co-ordinate system to calculate the baroclinic pressure gradient.

The use of a double sigma co-ordinate cannot solve all the limitations of the sigma grids. However, it can minimise the problems associated with the drying processes in intertidal areas and the errors associated with the density gradients in flows where there is a narrow thermocline with small vertical

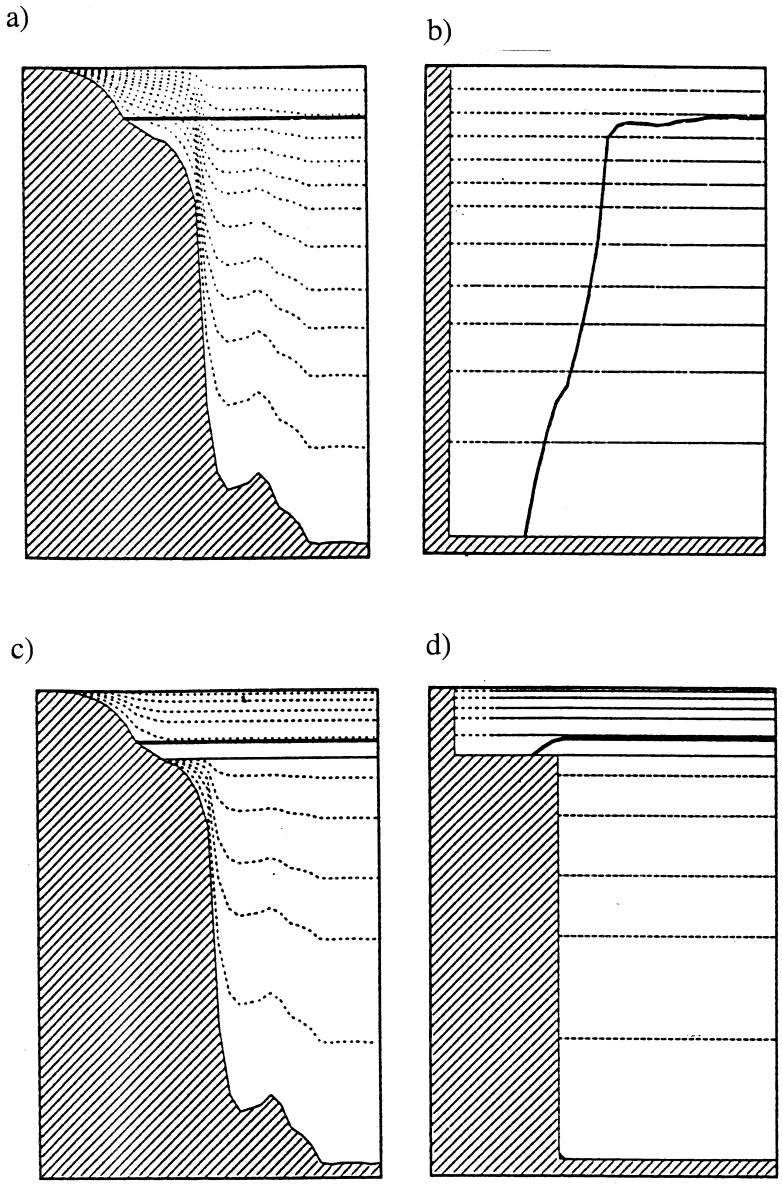

Fig. 2. Iso-σ-lines and idealised thermocline in (a) real space and (b) in the sigma co-ordinate. Iso-σ-lines and idealised thermocline in (c) real space and (d) in the two-fold sigma co-ordinate, (adapted from Beckers, 1991).

gradients both upwards and downwards. In the case of continuous vertical gradients, the concept must be generalised to *n*-sigma domains. This concept has the advantages of the Cartesian co-ordinates while still being able to represent correctly the bottom shear stress and the Coriolis term near the bottom.

3. Suspended sediment transport model

3.1. The transport equation

The cohesive sediment transport is governed by a 3D advection–diffusion equation where the vertical advection includes the particle settling velocity. In its

conservative form, the equation can be written as (Cancino and Neves, 1994a,b; 1995):

$$\frac{\partial(C)}{\partial t}+\frac{\partial(uC)}{\partial x}+\frac{\partial(vC)}{\partial y}+\frac{\partial((w+W_s)C)}{\partial z}=\frac{\partial}{\partial x}\left(\varepsilon_x\frac{\partial C}{\partial x}\right)+\frac{\partial}{\partial y}\left(\varepsilon_y\frac{\partial C}{\partial y}\right)+\frac{\partial}{\partial z}\left(\varepsilon_z\frac{\partial C}{\partial z}\right), \quad (9)$$

where C is the suspended sediment concentration, t is time, x, y are the horizontal co-ordinates, z is the vertical co-ordinate, ε_x, ε_y, ε_z are the sediment mass diffusion coefficients, W_S is the sediment fall velocity, and u, v, w are the flow velocity components in x, y, z directions.

Conservative properties are assumed in Eq. (9). The total mass of suspended sediments can change only due to fluxes across the estuarine boundaries (open boundaries, free surface and bottom). The fluxes across the open boundaries and across the free surface are to be imposed using field data. The fluxes across the bottom interface are a function of the concentrations calculated by the model, of the hydrodynamics and of the bottom sediment properties. Numerically, horizontal transport is solved explicitly, while the vertical one (including settling) is solved implicitly, for numerical stability reasons.

In tidal flows, the horizontal transport is mainly advective. In a sigma co-ordinate, the vertical transport is mainly forced by settling velocity and vertical diffusion. The fluxes across the water–bottom interface make the vertical transport especially important. During high velocity periods, there are conditions for erosion and the material removed from the bottom is transported upwards by diffusion. During periods of slack water, turbulence intensity is reduced and vertical settling imposes a net downward movement with possible bottom deposition.

3.2. The turbulent closure

In estuarine tidal systems, the maximum velocity gradients are located near the bottom and so is the generation of turbulence. As a consequence, the random component of the velocity increases from the bottom to the surface. This type of evolution has been found in coastal waters during the sixties by Bowden and Howe (1963) and confirmed later in laboratory experiments (e.g., Nezu and Rodi, 1986) and also in the field (West and Shiono, 1988; French et al., 1993).

In stratified systems, there is an increase of the potential energy when the water from lower layers moves upwards (and consequently, water from upper layers moves downwards). This energy is taken out from the turbulent kinetic energy, reducing the turbulent intensity. Stratification can be measured by the Richardson number (R_i):

$$R_i=-\left(g(\partial\rho/\partial z)\right)/\left(\rho(\partial U/\partial z)^2\right). \quad (10)$$

This number compares the rate of change of the potential energy of water moving upwards and the production rate of turbulent kinetic energy. Smaller values of R_i correspond to higher diffusion capacity, whereas at values close to unity, vertical diffusion nearly vanishes.

In general it is considered that the properties contributing to the water density are temperature and salinity; R_i is calculated accordingly. Darbyshire and West (1993) argue that cohesive sediments can give a non-negligible contribution and that the differences often found in turbulent intensities during ebb and flood tides (e.g. West and Oduyemi, (1989) and French et al. (1993)) can be explained by the contribution of suspended matter to fluid density. This must be expected to be a major contribution to fluid mud formation.

All the experimental data obtained in estuarine systems have been explained without recurring to horizontal transport of turbulent properties. This means that local equilibrium can be assumed in estuaries. This should be expected based on the difference between vertical and horizontal length scales. In this situation a mixing length approach may be used to calculate eddy viscosity.

The hydrodynamic model used in estuarine applications considers a Prandtl mixing length hypothesis (Robert and Ouellet, 1987) corrected, in stratified flows, by the local Richardson number. The horizontal viscosity is calculated using Kolmogorov's theory (Nihoul, 1984). The length scale is the grid size of the model as a measure of the non-resolved eddies. Vertical diffusivity is assumed to be proportional to the vertical eddy viscosity.

3.3. The settling velocity

The vertical transport is due to vertical advection, particle settling or turbulent diffusion. The hydrodynamic model computes the vertical velocity and the turbulent diffusivity. The settling velocity depends on the gravitational forces, and on the vertical shear due to settling movement. The gravitational forces depend on the density of each individual particle (terrigenous or biological) forming flocs and on the floc porosity occupied by water.

The frictional forces depend on the form of the floc and on the Reynolds number of the surrounding flow during settling. For very small bodies, the flow is laminar and the ratio between the gravitational and the frictional force is proportional to the reciprocal of the diameter of the floc. So, the settling velocity is expected to increase with floc size. Unfortunately, larger flocs can have smaller density and there is no unique relation between floc size and settling velocity.

The probability of particles to aggregate into flocs depends on the probability of the particles to collide. This probability is proportional to the concentration, and also increases with the amplitude and frequency of the turbulent random movement. Aggregation is a reversible process. Flocs are fragile and, if submitted to shear, they can disaggregate. Because shear increases also with turbulence intensity the latter plays a double role in the aggregation process.

Concentration also plays a double role. It increases the probability of flocculation and so the settling velocity. Nevertheless, when the number of flocs moving downward is very large, there is an interaction between the flows around adjacent ones. In these conditions, the upward friction tends to increase and the particle velocity decreases. The concentration at which the settling velocity starts to decrease is known as the 'hindering settling concentration'.

The concentration and the turbulence intensity determine the probability of two particles to meet. To form a floc, the particles must collide but, in addition, they must adhere to each other. Gluing forces depend on the type of particles (some biological particles have adhesive surfaces), and also on the ionisation of the environment. The latter is a function of the salinity, however, there is no correlation relating salinity and flocculation. From field work (Wollast, 1986), there is clear evidence that an intensive flocculation occurs as soon as salinity reaches about 1‰ and is complete for values higher than 2.5‰.

Models representing cohesive sediment by a bulk concentration use a bulk settling velocity. If no information is available on the type of particles in the system and no evolution equation is solved for each class of flocs, then it is not possible to explicitly represent the flocculation processes in this type of correlation. The general correlation for the settling velocity in the flocculation range (11a) and in the hindered settling range (11b) is:

$$W_S = K_1 C^m \quad \text{for} \quad C < C_{HS}, \tag{11a}$$

$$W_S = K_1 C_{HS}^m \left[1.0 - K_2 (C - C_{HS})\right]^{m_1} \quad \text{for} \quad C > C_{HS}, \tag{11b}$$

where W_S (ms^{-1}) is the settling velocity, C (kg m^{-3}) is the concentration, and the subscript HS refers to the onset of the hindered settling (of about 2 to 5 kg m^{-3}). The coefficients K_1 (m^4 kg^{-1} s^{-1}) and K_2 (m^3 kg^{-1}) depend on the mineralogy of the mud and the exponents m and m_1 depend on particle size and shape.

Krone (1962), based on the kinetics of flocculation, proposed a theoretical value for m equal to $4/3$. Mehta (1986) found, experimentally, values varying between 1 and 2. In expression (11b), the exponent m_1 is usually taken as 4.65 for small particles and 2.32 for large particles (Dyer, 1986). To ensure that Eqs. (11a) and (11b) are dimensionally correct, both m and m_1 should be 1.

This type of correlation is adequate for models that calculate a bulk concentration. In 3D hydrodynamic models, the intensity of turbulence is calculated and a more complex correlation could be used. That type of correlation is not yet available. However, the situation is expected to improve, due to advances in measuring techniques and modelling.

3.4. Bottom interface module

Although there is evidence that matter is continuously deposited and removed from the bottom (e.g., Stanford and Halka, 1993), most models follow Einstein (1950) and consider that the two processes cannot occur simultaneously. In such models, it is

assumed that, when bottom friction is smaller than a critical value for deposition, there is addition of matter to the bottom, and, when the bottom shear is higher than a minimum value, erosion occurs. Between those values, erosion and deposition balance each other. In fact, only very recently has it been possible to measure the downward and upward movement of particles at the bottom interface. In former times, the best that could be achieved was to measure the net erosion or deposition as a function of the bottom shear. Both formulations can easily be included in the same model. In this work, the traditional approach was adopted because it is much easier to find data in the literature to specify the parameters.

3.4.1. The erosion model

Erodibility of a cohesive bed is driven by shear, but also depends on bottom cohesive nature, which in turn depends, in a poorly understood way, on clay mineralogy and on the geochemistry and microbiological processes occurring in the bottom. Some authors argue that it should also depend on the salinity (Hayter and Mehta, 1986). However, no dependency laws have yet been advanced.

Again, a useful correlation must depend only on the variables calculated by the model and on parameters. The erosion algorithm used in this work is based on the classical approach of Partheniades, (1965). Erosion occurs when the ambient shear stress exceeds the threshold of erosion. The flux of eroded matter is given by:

$$\frac{\partial M_E}{\partial t} = E\left(\frac{\tau}{\tau_E} - 1\right) \qquad \text{for} \quad \tau > \tau_E, \tag{12a}$$

$$\frac{\partial M_E}{\partial t} = 0 \qquad \text{for} \quad \tau < \tau_E, \tag{12b}$$

where τ is the bed shear stress, τ_E is a critical shear stress for erosion and E is the erosion constant (kg m^{-2} s^{-1}).

The parameter E (Eq. 12a) depends on the physico-chemical characteristics of bottom sediment. In the Western Scheldt, Mulder and Udink, (1991) used 5×10^{-5} kg m^{-2} s^{-1}. As a general rule, bottom-sediments are a mixture of cohesive and non-cohesive sediments; this parameter must also account for that and so a gradient must be expected in the estuary.

Critical shear stress for erosion is a function of the degree of compaction of bottom sediments measured by the dry density of the bottom sediments: ratio between the mass of sediment (after extraction of the interstitial water at 105°C) and its initial volume.

Stephens et al. (1992), based on the formulations proposed by Delo (1988), used:

$$\tau_E = A_1(\rho_d)^{E_1}, \tag{13}$$

where ρ_d (kg m^{-3}) is dry density of bed sediments, and A_1 (m^2 s^{-2}) and E_1 are coefficients depending on mud type.

This equation is dimensionally correct only for $E_1 = 1$. Nevertheless, Stephens et al. (1992) calibrated their model with $A_1 = 0.0012$ m^2 s^{-2} and $E_1 = 1.2$. This is a critical point when a compaction model is used, otherwise, this correlation becomes an indirect means of imposing a critical shear stress for erosion knowing the bed sediment dry density, much easier to measure. The deviation of the coefficient E_1 from unity can be seen as a measure of the error of the input data.

3.4.2. The deposition model

The deposition algorithm, like the erosion algorithm, is based on the assumption that deposition and erosion never occur simultaneously. An algorithm was first proposed by Krone (1962) and later on modified by Odd and Owen, (1972). The algorithm is based on the assumption that a particle reaching the bottom has a probability of remaining there that varies between 0 and 1 as the bottom shear stress varies between its upper limit for deposition and zero, respectively. Deposition is calculated as the product of the settling flux and the probability of a particle to remain on the bed:

$$\frac{\partial M_D}{\partial t} = C_B(W_S)\left(1 - \frac{\tau}{\tau_D}\right) \qquad \text{for} \quad \tau > \tau_D, \tag{14a}$$

$$\frac{\partial M_D}{\partial t} = 0 \qquad \text{for} \quad \tau < \tau_D, \tag{14b}$$

where τ_D is the critical stress for deposition and subscript B means ‘at the sediment–water interface’.

The critical shear stress for deposition, τ_D, depends mainly on the size of the flocs. Bigger flocs have higher probability of remaining on the bed than smaller flocs. Nevertheless, previous work suggest that a constant value is a reasonable approximation. Based on laboratory experiments with natural mud from the Western Scheldt, Winterwerp et al. (1991) found $\tau_D = 0.2$ N m^{-2}. For the Gironde, Li et al. (1994) used values in the range 0.3–0.5 N m^{-2}.

4. Concluding remarks

In this paper, a 3D baroclinic model is presented for hydrodynamics and cohesive sediment transport in tidal estuaries. The model employs a double sigma co-ordinate for vertical discretisation and a classical approach for sediment transport. The use of a double sigma coordinate has improved the stability properties of the model in intertidal areas and can be generalized to a larger number of sigma domains very easily. The inconsistencies in terms of dimensions in the correlations describing settling velocity and exchanges with the bottom suggest that some more experimental work is still needed on this subject.

The present situation can be understood by taking into account that, when solving an equation with several terms, the global error has a contribution from each term. So, the optimal strategy to minimize the global error is the simultaneous minimization of every error. Until recently, models were of 1D or 2D type and were unable to describe the vertical processes without resorting to highly simplified hypotheses. The present stage of development of 3D models will stimulate the improvement of the correlations used in a sediment transport model, as well as the collection of the data needed to characterise the bottom sediments. The development of non-disturbing and remote sensing measuring techniques will also simplify field work.

Mathematical models can give a very useful contribution to that development, by providing a detailed description of the hydrodynamic field—including the wave induced circulation—and a continuous test of hypotheses.

Acknowledgements

Most of this work was undertaken as a part of the project 'Biogeochemistry of the *MA*ximum *TUR*bidity Zone in *E*stuaries' (MATURE), funded by the Commission of the European Communities, Environment Programme under contract no. 910357. The first author gratefully acknowledges the financial support of the Programa Ciência/JNICT and is indebted to Professor António Falcão for encouragement and kind help.

References

Ariathurai, R., Krone, R.B., 1976. Finite element model for cohesive sediment transport. J. Hydr. Div., ASCE 102 (HY3), 323–338.

Bagnold, R.A., 1936. The movement of desert sand. Proc. R. Soc. London A 157, 594–620.

Bagnold, R.A., 1937. The size-grading of sand by wind. Proc. R. Soc. London A 163, 250–264.

Beckers, J.M., 1991. Application of the GHER 3D general circulation model to the Western Mediterranean. In: J. Mar. Syst. 1 Elsevier, Amsterdam, pp. 315–332.

Blumberg, A.F., Mellor, G.L., 1983. Diagnostic and prognostic numerical circulation studies of the South Atlantic Bight. J. Geophys. Res. 88, 4579–4592.

Bowden, K.F., Howe, M.R., 1963. Observations of turbulence in a tidal current. Journal of Fluid Mechanics 17, 271–284.

Cancino, L., Neves, R., 1994a. Numerical modelling of three-dimensional cohesive sediment transport in an estuarine environment. In: Bélorgey, M., Rajaona, R.D., Sleath, J.F.A. (Eds.), Sediment Transport Mechanisms in Coastal Environments and Rivers. World Scientific, pp. 107–121.

Cancino, L., Neves, R., 1994b. 3D-numerical modelling of cohesive suspended sediment in the Western Scheldt estuary (The Netherlands). Netherlands Journal of Aquatic Ecology 28 (3–4), 337–345.

Cancino, L., Neves, R., 1995. Three-dimensional model system for baroclinic estuarine dynamics and suspended sediment transport in a mesotidal estuary. In: Computer Modelling of Seas and Coastal Regions. Computational Mechanics Publications, pp. 353–360.

Darbyshire, E.J., West, J.R., 1993. Turbulence and cohesive sediment transport in the Parrett estuary. In: Clifford, N.J., French, J.R., Hardisty, J. (Eds.), Turbulence: Perspectives and Sediment Transport. Wiley.

De Kok, J.M., Salden, R., Rozendaal, I.D.M., Blokland, P., Lander, J., 1995. Transport path of suspended matter along the Dutch coast. In: Modelling of Seas and Coastal Regions. Computational Mechanics Publications, pp. 75–86.

De Vries, M., Klaassen, G.J., Striksma, N., 1989. On the use of

movable bed models for rivers problems: state of the art, Symp. River Sedimentation, Beijing, China.

Delleersnijder, E., Beckers, J.-M., 1992. On the use of the sigma-coordinate system in regions of large bathymetric variations. J. Mar. Syst. 3, 381–390.

Delo, E.A., 1988. Estuarine Muds Manual. Report No. SR 164. Hydraulics Research, Wallingford, UK, 64 pp.

Dyer, K.R., 1986. Coastal and Estuarine Sediment Dynamics. Wiley-Interscience, 342 pp.

Dyer, K.R., Evans, E.M., 1989. Dynamics of turbidity maximum in a homogeneous tidal channel. J. Coastal Research, 23–30, Special Issue No.5, Fort Lauderdale, FL.

Einstein, H.A., 1950. The bedload function for sediment transportation in open channel flows. Soil Cons. Serv. US Dept. Agric. Tech. Bull. 1026, 78 pp.

Einstein, H.A., Chien, N., 1955. Effects of heavy sediment concentration near bed on velocity and sediment distribution, MRD Series Rep.8. Inst. Eng. Research, Univ. of Calif., Berkeley.

French, J.R., Clifford, N.J., Spence, T., 1993. High frequency flow and suspended sediment measurements in a tidal wetland channel. In: Clifford, N.J., French, J.R., Hardisty, J. (Eds.), Turbulence: Perspectives and Sediment Transport. Wiley.

Hayter, E.J., Mehta, A.J., 1986. Modelling cohesive sediment transport in estuarine waters. Appl. Math. Modelling 10, 294–303.

Katopodi, I., Ribberink, J.S., 1992. Quasi-3D modelling of suspended sediment transport by currents and waves. Coastal Engineering 18, 83–110.

Krone, R.B., 1962. Flume Studies of the Transport in Estuarine Shoaling Processes. Hydr. Eng. Lab., Univ. of Berkeley, CA, USA, 110 pp.

Li, Z.H., Nguyen, K.D., Brun-Cottan, J.C., Martin, J.M., 1994. Numerical simulation of the turbidity maximum transport in the Gironde estuary (France). Oceanologica Acta.

Mehta, A.J., 1986. Characterisation of cohesive sediment properties and transport processes in estuaries. In: Mehta, A.J. (Ed.), Estuarine Cohesive Sediment Dynamics 14 Springer-Verlag, Berlin, pp. 290–325.

Mulder, H.P.J., Udink, C., 1991. Modelling of cohesive sediment transport. A case study: the western Scheldt estuary. In: Edge, B.L. (Ed.), Proceedings of the 22nd International Conference on Coastal Engineering. American Society of Civil Engineers, New York, pp. 3012–3023.

Nezu, Rodi, 1986. Open channel flow measurements with a laser Doppler anemometer. Journal of Hydraulic Engineering, American Society of Civil Engineers 112, 335–355.

Nihoul, J.C.J., 1984. A three-dimensional general marine circulation model in a remote sensing perspective. Annales Geophysicae 2–4, 433–442.

O'Connor, B.A., 1971. Mathematical Model for Sediment Distribution. Proc. 14th IAHR Conf., Paper D23, Paris, France.

O'Connor, B.A., Nicholson, J.A., 1988. Mud transport modelling. In: Dronkers, J., van Leussen, W. (Eds.), Physical Processes in Estuaries. Springer-Verlag, pp. 532–544.

Odd, N.V.M., Owen, M.W., 1972. A two-layer model of mud transport in the Thames estuary. In: Proceedings. Institution of Civil Engineers, London, pp. 195–202.

Partheniades, E., 1965. Erosion and deposition of cohesive soils. J. Hydr. Div., ASCE 91 (HY1), 105–139.

Phillips, N.A., 1957. A coordinate system having some spacial advantages for numerical forecasting. J. Meteorol. 14, 184–186.

Robert, J.L., Ouellet, Y., 1987. A three-dimensional finite element model for the study of steady and non-steady natural flows. In: Nihoul, J.C.J., Jamart, B.M. (Eds.), Elsevier Oceanography Series 45, pp. 359–372.

Ross, M.A., Mehta, A.J., 1989. On the mechanics of lutoclines and fluid mud. J. Coastal Res. 5, 51–62.

Santos, A.J., 1995. 3D Hydrodynamic Model for Estuarine and Oceanic Circulation, (in Portuguese). PhD Thesis, I.S.T., Portugal.

Santos, A.J, Neves, R., 1991. Radiative artificial boundaries in ocean barotropic models. In: Arcilla, A.S. (Ed.), Proceedings of the 2nd Int. Conf. on Computer Modelling in Ocean Engineering, Barcelona, pp. 373–383.

Sheng, Y.P., 1986. Modelling bottom boundary layer and cohesive sediment dynamics in estuarine and coastal waters. In: Mehta, A.J. (Ed.), Estuarine Cohesive Sediment Dynamics 14 Springer-Verlag, Berlin, pp. 360–400.

Smith, T.J., Kirby, R., 1989. Generation, stabilisation and dissipation of layered fine sediment suspensions. J. Coastal Res. 5, 63–73.

Stanford, L.P., Halka, J.P., 1993. Assessing the paradigm of mutually exclusive erosion and deposition of mud with examples from upper Chesapeake Bay. Mar. Geol. 114, 37–57.

Stephens, J.A., Uncles, R.J., Barton, M.L., Fitzpatrick, F., 1992. Bulk properties of intertidal sediments in a muddy macrotidal estuary. Mar. Geol. 103, 15 pp.

West, J.R., Oduyemi, K.O.K., 1989. Turbulence measurements of suspended solids concentration in estuaries. Journal of Hydraulic Engineering, American Society of Civil Engineers 115, 457–474.

West, J.R., Shiono, K., 1988. Vertical turbulent mixing processes on ebb tides in partially mixed estuaries. Estuarine, Coastal and Shelf Science 20, 51–66.

Winterwerp, J.C., Cornelisse, J.M., Kuijper, C., 1991. The behaviour of mud from the Western Scheldt under tidal conditions. Delft Hydraulics, The Netherlands, Rep. z161–37/HW/paper1.wm, 14 pp.

Wollast, R., 1986. The Scheldt estuary. In: Salomon, W., Bayne, B.L., Duursma, E.K., Forstner, U. (Eds.), Pollution of the North Sea. An Assessment. Springer-Verlag, pp. 183–193.